arXiv:2411.01356v1 [astro-ph.EP] 2 Nov 2024

Origins of Super Jupiters: TOI-2145b Has a Moderately Eccentric and Nearly Aligned Orbit

Jiayin Dong [ID],[1,2,*] Ashley Chontos [ID],[3,†] George Zhou [ID],[4] Gudmundur Stefansson [ID],[5] Songhu Wang [ID],[6]
Chelsea X. Huang [ID],[4] Arvind F. Gupta [ID],[7,‡] Samuel Halverson [ID],[8] Shubham Kanodia [ID],[9,§] Jacob K. Luhn [ID],[10,8,¶]
Suvrath Mahadevan [ID],[11,12,**] Andrew Monson [ID],[13] Jaime A. Alvarado-Montes [ID],[14,15] Joe P. Ninan [ID],[16]
Paul Robertson [ID],[10,††] Arpita Roy [ID],[17] Christian Schwab [ID],[14,15] and Jason T. Wright [ID][11,12,18]

[1]Center for Computational Astrophysics, Flatiron Institute, 162 Fifth Avenue, New York, NY 10010, USA
[2]Department of Astronomy, University of Illinois at Urbana-Champaign, Urbana, IL 61801, USA
[3]Department of Astrophysical Sciences, Princeton University, 4 Ivy Lane, Princeton, NJ 08540, USA
[4]University of Southern Queensland, Centre for Astrophysics, West Street, Toowoomba, QLD 4350 Australia
[5]Anton Pannekoek Institute for Astronomy, 904 Science Park, University of Amsterdam, Amsterdam, 1098 XH
[6]Department of Astronomy, Indiana University, Bloomington, IN 47405, USA
[7]U.S. National Science Foundation National Optical-Infrared Astronomy Research Laboratory, 950 N. Cherry Ave., Tucson, AZ 85719, USA
[8]Jet Propulsion Laboratory, California Institute of Technology, 4800 Oak Grove Drive, Pasadena, California 91109
[9]Carnegie Science Earth and Planets Laboratory, 5241 Broad Branch Road, NW, Washington, DC 20015, USA
[10]Department of Physics & Astronomy, The University of California, Irvine, Irvine, CA 92697, USA
[11]Department of Astronomy & Astrophysics, 525 Davey Laboratory, Penn State, University Park, PA, 16802, USA
[12]Center for Exoplanets and Habitable Worlds, 525 Davey Laboratory, Penn State, University Park, PA, 16802, USA
[13]Steward Observatory, University of Arizona, 933 N. Cherry Ave, Tucson, AZ 85721, USA
[14]School of Mathematical and Physical Sciences, Macquarie University, Balaclava Road, North Ryde, NSW 2109, Australia
[15]The Macquarie University Astrophysics and Space Technologies Research Centre, Macquarie University, Balaclava Road, North Ryde, NSW 2109, Australia
[16]Department of Astronomy and Astrophysics, Tata Institute of Fundamental Research, Homi Bhabha Road, Colaba, Mumbai 400005, India
[17]Astrophysics & Space Institute, Schmidt Sciences, New York, NY 10011, USA
[18]Penn State Extraterrestrial Intelligence Center, 525 Davey Laboratory, Penn State, University Park, PA, 16802, USA

ABSTRACT

Super Jupiters are giant planets with several Jupiter masses. It remains an open question whether these planets originate with such high masses or grow through collisions. Previous work demonstrates that warm super Jupiters tend to have more eccentric orbits compared to regular-mass warm Jupiters. This correlation between mass and eccentricity may indicate that planet-planet interactions significantly influence the warm giant planet demographics. Here we conducted a detailed characterization of a warm super Jupiter, TOI-2145b. This analysis utilized previous observations from TESS and Keck/HIRES, enhanced by new Rossiter-McLaughlin effect data from the NEID spectrometer on the 3.5 m WIYN Telescope. TOI-2145b is a $5.68^{+0.37}_{-0.34}\,M_{\rm Jup}$ planet on a moderate eccentricity ($e = 0.214^{+0.014}_{-0.014}$), 10.26-day orbit, orbiting an evolved A-star. We constrain the projected stellar obliquity to be $\lambda = 6.8^{+2.9}_{-3.8}{}^\circ$ from two NEID observations. Our N-body simulations suggest that the formation of super Jupiter TOI-2145b could involve either of two scenarios: a high initial mass or growth via collisions. On a population level, however, the collision scenario can better describe the mass-eccentricity distribution of observed warm Jupiters.

1. INTRODUCTION

Corresponding author: Jiayin Dong
jdong@flatironinstitute.org

* Flatiron Research Fellow
† Henry Norris Russell Fellow
‡ NOIRLab Postdoctoral Fellow
§ Carnegie EPL Fellow
¶ NASA Postdoctoral Program Fellow
** NEID Principal Investigator
†† NEID Instrument Team Project Scientist

It has long been recognized that a positive correlation between planetary mass and orbital eccentricity exists among radial velocity discovered giant planets (Butler et al. 2006; Wright et al. 2009). These giant planets have orbital periods ranging from a few days to several thousand days and projected mass ($M_p \sin i$) from roughly 0.1 to 10 $M_{\rm Jup}$. This positive mass-eccentricity correlation has been interpreted as a result of planet-planet interactions, such as scatterings and collisions (e.g., Ford & Rasio 2008; Chatterjee et al. 2008; Jurić & Tremaine 2008; Frelikh et al. 2019).

Recently, a similar trend has been reported in the population of transiting warm Jupiters (Gupta et al. 2024). Close-in giant planets with masses ranging from 0.3 to 15 $M_{\rm Jup}$ and orbital periods between 10 and 365 days exhibit a mass-dependent eccentricity distribution. Unlike many planets discovered via radial velocity, these transiting giant planets do not suffer from the mass degeneracy due to the unknown orbital inclination angle. Warm Jupiters less massive than 2 $M_{\rm Jup}$ tend to have circular or low eccentricity orbits, while those more massive than 2 $M_{\rm Jup}$– i.e., super-Jupiters–exhibit a broad range of eccentricities. This mass-eccentricity dependence likely explains the bimodal eccentricity distribution observed in warm Jupiters (Dong et al. 2021), where the observed low-e component represents the low-mass warm Jupiters, while the high-e component represents the super, warm Jupiters.

Planet-planet interactions likely play a role in shaping the mass and eccentricity distribution of warm Jupiters, shedding light on their origins. Among these, the formation of super Jupiters is particularly interesting. These massive planets can either form through collisions between multiple lower-mass giant planets, resulting in low eccentricity and mutual inclinations, or they may be born massive, with their eccentricity and inclination further excited by companions. It is also unclear whether the origin of super Jupiters depends on stellar properties. To better understand this feature, we conduct a detailed characterization of a warm, super Jupiter, TOI-2145b. The planet was first discovered and had its orbital properties confirmed by Rodriguez et al. (2023), and later had its properties refined by Chontos et al. (2024). TOI-2145b is a 10.3-day period, 5.7 Jupiter-mass planet orbiting a retired A-star ($M_\star = 1.71 \pm 0.04$ $M_\odot$, $\log g = 3.79 \pm 0.02$). The planet has a moderate orbital eccentricity of 0.22 but unknown stellar obliquity.

The underlying assumption of planet-planet interactions as the cause of the observed mass-eccentricity trend is that dynamical interactions primarily occur at the semimajor axes of the planets observed today. Whether giant planets migrated inward or formed in situ, post-formation dynamical interactions shape the observed trend (Wu et al. 2023). Under such assumptions, planet-planet interactions could excite mutual inclinations between planets, but not significantly so

($i_{\rm mutual} < 40°$; Anderson et al. 2020). This is consistent with the trend of low stellar obliquity observed in the warm Jupiter population around single stars (e.g., Rice et al. 2022; Dong et al. 2022; Radzom et al. 2024; Wang et al. 2024). Some warm Jupiters, such as TOI-1859b (Dong et al. 2023), are found in misaligned orbits; however, their host stars often have distant stellar companions, with projected distances around 2400 au in this case. The impact of stellar companions on planet formation remains unclear.

In this work, we present the Rossiter-McLaughlin (RM) effect measurements of TOI-2145b (HIP 86040) using the high-resolution NEID spectrograph. In Section 2, we summarize previous *TESS* and HIRES observations. In Sections 3 and 4, we model and present the stellar and planetary properties of TOI-2145b, respectively, combining the *TESS* transits, HIRES radial velocity, and NEID RM-effect and Doppler Tomography signals. We also search for external companions of TOI-2145b using *Gaia* and *Hipparcos* astrometry. Lastly, in Section 5, we discuss the properties of the TOI-2145 system and its implications for warm Jupiter origins.

2. OBSERVATIONS

2.1. *Summary of Previous Observations*

The planet TOI-2145b was detected by the Transiting Exoplanet Survey Satellite (*TESS*; Ricker et al. 2014). Rodriguez et al. (2023) first discovered and confirmed its planetary nature using ground-based photometry from the *TESS* Follow-up Observing Program (TFOP; Collins et al. 2018), high-resolution adaptive optics (AO) imaging with the PHARO instrument (Hayward et al. 2001) on the Palomar 200-inch telescope and ShARCS on the Shane 3 m telescope at Lick Observatory, and high-resolution spectroscopy with the Tillinghast Reflector Echelle Spectrograph (TRES; Fűrész 2008) on the 1.5 m Tillinghast Reflector at the Fred Lawrence Whipple Observatory, as well as the MINERVA North telescope array and KiwiSpec Spectrograph (Swift et al. 2015; Wilson et al. 2019) at Whipple Observatory. The planet's mass and orbit have been constrained. Later, Chontos et al. (2024) refined the planet's mass and orbital parameters using the HIRES Spectrograph (Vogt et al. 1994) on the Keck 10-meter telescope on Mauna Kea, Hawaii.

Here, we briefly summarize the observations used in our modeling. The star has been observed in six sectors of *TESS* —Sectors 25, 26, 40, 52, 53, and 79. As this manuscript was being prepared, the Quick Look Pipeline (QLP; Huang et al. 2020a,b) reduced light curves cover Sectors 25, 26, 40, 52, and 53. Notably, the observing cadence decreases from 30 minutes in Sectors 25 and 26 to 10 minutes in Sectors 40, 52, and 53. The Science Processing Operations Center (SPOC; Jenkins et al. 2016) reduced light curves are available for Sectors 26, 40, 52, 53, and 79, all with an observ-

ing cadence of 2 minutes. Additionally, 20-second cadence data is available for Sector 79. We use the 2-minute SPOC light curves from Sectors 26, 40, 52, 53, and 79, along with the QLP light curves from Sector 25, for the joint fit. Forty HIRES spectra were taken from August 25, 2020, to May 13, 2022, spanning 1.7 years (Chontos et al. 2024). The median HIRES radial velocity (RV) uncertainty is $5.2\,\mathrm{m\,s^{-1}}$, although this number could be underestimated given the star's large $v\sin i_\star$. The HIRES RVs are used for the joint fit with a treatment of the underestimated RV uncertainties.

2.2. *Transit Spectroscopic Observation*

Two transit spectroscopy observations were taken by the NEID spectrograph (Schwab et al. 2016; Halverson et al. 2016) on the WIYN 3.5 m telescope at the Kitt Peak National Observatory (KPNO) in Arizona, USA. The NEID spectrograph is a highly stabilized (Robertson et al. 2019; Stefansson et al. 2016), fiber-fed (Kanodia et al. 2018, 2023) spectrograph with a resolving power of $R \approx 110,000$ in high-resolution (HR) mode and has wavelength coverage from 380 nm to 930 nm. The first NEID RM-effect visit occurred on May 26, 2023. The observation began at 03:10 UT and lasted 6.3 hours. We obtained 35 spectra, each with a 10-minute exposure time, in HR mode, covering approximately 69% of the transit. The second NEID visit took place on July 6, 2023. The observation started at 02:30 UT and lasted 7.5 hours. We obtained 41 spectra, each with a 10-minute exposure time, in HR mode, covering approximately 77% of the transit.

The NEID data reduction has been performed using three different pipelines: the standard NEID Data Reduction Pipeline v1.3.0 (NEID-DRP), the SERVAL Pipeline (Zechmeister et al. 2018; Stefànsson et al. 2022), and Doppler Tomography (DT; Collier Cameron et al. 2010). The reduced data are presented in Figure 2 and Figure 3, respectively. The NEID-DRP pipeline utilizes the cross-correlation function (CCF) technique to extract the radial velocities. Due to a minor bug in the NEID-DRP that causes the computed RV error bars to be systematically overestimated for certain targets that have significantly discrepant systemic velocities relative to literature values, we recalculated the RV errors independently using the DRP-derived CCFs using standard techniques Boisse et al. (2010). The median NEID-DRP RV uncertainties are $15.4\,\mathrm{m\,s^{-1}}$ and $11.9\,\mathrm{m\,s^{-1}}$ for the first and second visits, respectively. The SERVAL pipeline initially builds a stellar template from the NEID observations and uses least-squares fitting to extract the radial velocities. The median RV uncertainties out of the SERVAL pipeline are $9.5\,\mathrm{m\,s^{-1}}$ and $7.0\,\mathrm{m\,s^{-1}}$ for the first and second visits, respectively. Lastly, DT models the line profile variations induced by the transiting shadow of the planet. The line profiles are derived via a least-squares deconvolution (LSD; Donati et al. 1997)

of each observation against a non-rotating synthetic template generated from the ATLAS9 model atmospheres (Castelli & Kurucz 2004). An average line profile is then removed from each observation, and the residuals are modeled for the planetary transit signature.

3. STELLAR PROPERTIES

We derive the stellar parameters following the procedures described in Section 4 of Chontos et al. (2024). We first use SpecMatch-Synth (Petigura 2015) to derive the stellar effective temperature (T_{eff}), metallicity ([Fe/H]), and surface gravity ($\log g$) of the star. We then model the spectral energy distribution (SED) and the MESA Isochrones and Stellar Tracks (MIST; Choi et al. 2016; Dotter 2016) to derive the age, mass, and radius of the star using isoclassify (Huber et al. 2017). The stellar parameters T_{eff} and [Fe/H] from SpecMatch are used as inputs for the model. We include the Johnson B and V magnitudes from the APASS catalog (Henden et al. 2015), 2MASS J, H, and K_s magnitudes (Skrutskie et al. 2006), and the *Gaia* DR3 G, R_p, and B_p magnitudes (Gaia Collaboration et al. 2021) to fit the SED. The *Gaia* DR3 parallax (Gaia Collaboration et al. 2021) is used to determine the distance to the star. The results are summarized in Table 1.

The star has four blocks of *TESS* data, separated by 1-year or 2-year gaps. To avoid the dominance of the window function in the periodogram for the entire dataset, we calculate the periodogram of the light curve piece by piece. Interestingly, the Sectors 25–26 *TESS* data from 2019 show a periodicity of 5.9 days, whereas Sector 40 in 2020 shows 7.0 days, Sectors 52–53 in 2021 show 5.1 days, and Sector 79 in 2024 shows show 3.4 days. The period detected in Sector 79 is shorter than those in the other sectors, which might indicate that it is an alias of 6.8 days. We attribute the lack of consistency in the star's periodicity to its multiple spot complexes. The rotation periods between 5–7 days correspond to an equatorial velocity of 20–$28\,\mathrm{km\,s^{-1}}$. As a sanity check, this velocity is above the projected rotational velocity of $\sim 18\,\mathrm{km\,s^{-1}}$, and the deviation may indicate a stellar inclination apart from 90 degrees. Although the star is evolved, existing *TESS* data did not detect the oscillation modes of TOI-2145. According to the scaling relation for the oscillation frequency $\nu_{\mathrm{max}} = 3100\,\mu\mathrm{Hz}\,(M/M_\odot)(R/R_\odot)^{-2}(T_{\mathrm{eff}}/T_{\mathrm{eff},\odot})^{-0.5}$ (Chaplin et al. 2019), TOI-2145 should oscillate at ~ 58 cycles per day, a signal that is not detected in the *TESS* data.

4. PLANET PROPERTIES

4.1. *TTV Modeling*

Since both of our RM-effect measurements captured only a partial transit of TOI-2145b, understanding the transit-timing variation (TTV) properties of the planet is crucial for robust stellar obliquity inference. We modeled the *TESS* transits,
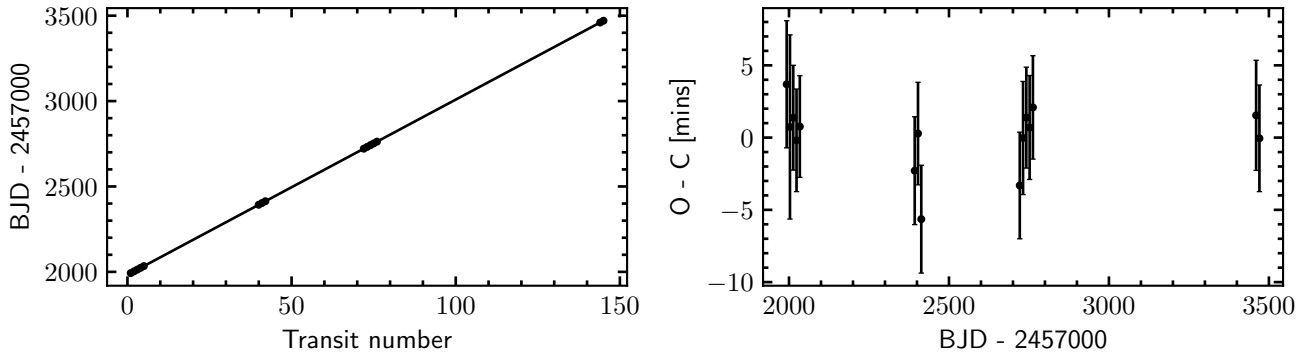
Figure 1. Transit-timing variation on TOI-2145b. The planet exhibits a transit timing variation of less than 5 minutes over a 4-year baseline, with a typical mid-transit time uncertainty of 2.7 minutes.

treating each transit's mid-transit time as a free parameter. We then fitted a linear line to the mid-transit times, deriving the orbital period, one reference transit epoch, and TTV signals. Benefiting from multiple sectors of *TESS* observations over four years, we modeled 15 transits of TOI-2145b over this period. The results are shown in Figure 1. The scatter in transit timing variations is less than 5 minutes, with the median mid-transit time uncertainty of about 3.7 minutes. No obvious TTV patterns have been detected in existing *TESS* observations. We derive the orbital period $P = 10.261129 \pm 0.000009$ in days and reference transit epoch $T_C = 1982.49664 \pm 0.00067$ in BJD $- 2457000$.

Because of the lack of TTVs, in the global modeling to be discussed in the next section, we model P and T_C without individually modeling each mid-transit time. The derived orbital period and reference transit epoch are well agree with those obtained from the TTV modeling, within 1σ consistency.

4.2. *Global Modeling: Transit+RV+RM-effect*

As the main result of this work, we present the joint model *TESS* transit, HIRES radial velocities, and NEID RM-effect signals to derive the planetary and orbital properties of TOI-2145b. We use the exoplanet package (Foreman-Mackey et al. 2019; Foreman-Mackey et al. 2021) to build the model and perform the Markov chain Monte Carlo (MCMC) using the PyMC package (Oriol et al. 2023).

We run three different models, all including *TESS* and HIRES data, but one with the RM-effect signal reduced by NEID-DRP, one by SERVAL, and one by DT. The model includes the following planetary and orbital parameters:

- P: orbital period
- T_C: reference transit epoch
- b: impact parameter
- $R_p/R_\star$: planet-to-star radius ratio
- M_p: planet mass
- e: orbital eccentricity

- ω: argument of periapse
- λ: projected stellar obliquity

Among these free parameters, a uniform prior is used on P, T_C, b, and λ, a log-uniform prior is used on $R_p/R_\star$ and M_p, and a unit disk vector is used on $\sqrt{e}\cos\omega$ and $\sqrt{e}\sin\omega$, where both e and ω are uniformly distributed. For both the NEID-DRP and SERVAL fittings, we use the Hirano et al. (2011) model to calculate the RV anomaly due to the RM effect. In addition to the quadratic limb darkening coefficients (Kipping 2013a) for the *TESS* transits, we model another pair for the NEID observations. Additionally, we model RV jitters, $\sigma_{\rm RV,DRP}$ and $\sigma_{\rm RV,SERVAL}$, in log-uniform space as free parameters added to both HIRES and NEID RV uncertainties. Lastly, we model the projected stellar rotation velocity $v\sin i_\star$ using a Normal prior derived from the spectra. Independently, we perform the joint modeling of the *TESS* transit, HIRES RV, and NEID DT signals. We model the planetary shadow at each time snapshot as a Gaussian profile that is broadened by the instrumental resolution and macroturbulence of the host star $v_{\rm marco}$, which follows a prior uniformly between 0 and $10\,{\rm km\,s^{-1}}$. The center of the velocity profile depends on the projected stellar obliquity λ and will be inferred. For each model, we begin with an optimization and then run the MCMC with 5000 tuning steps and 3000 draws with 4 independent chains. To check the convergence and sampling efficiency, we use the Gelman-Rubin diagnostic ($\hat{\mathcal{R}}$ convergence to 1; Gelman & Rubin 1992) and the effective sample size (ESS; Gelman et al. 2014). All three models have passed the convergence test. A summary of the results can be found in Table 1 and Figure 2 and 3.

The NEID-DRP and SERVAL pipelines infer $\lambda = 9.0^{+15.6\circ}_{-13.4}$ and $\lambda = 10.9^{+11.8\circ}_{-11.5}$, respectively, while the DT signal infers $\lambda = 6.8^{+2.9\circ}_{-3.8}$. The three inferred projected stellar obliquities are consistent with each other, ruling out a polar or retrograde orbit of TOI-2145b. Because of the high dimensionality of the DT signal, the DT model provides the tightest constraint on the projected stellar obliquity λ. We adopt the DT results for the discussion of this work.
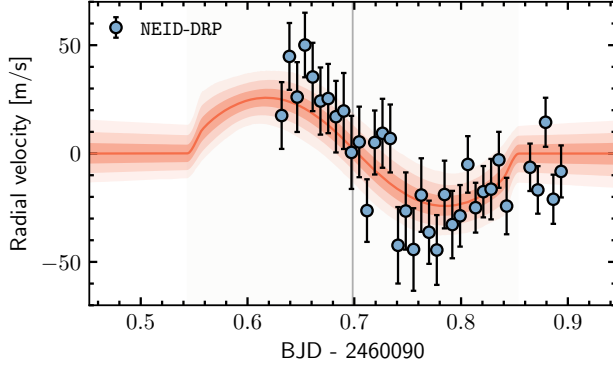
(a) In-transit RVs reduced by the NEID-DRP v1.3.0 pipeline, which infer $\lambda = 9.0^{+15.6\circ}_{-13.4}$. The orbit trend has been subtracted.
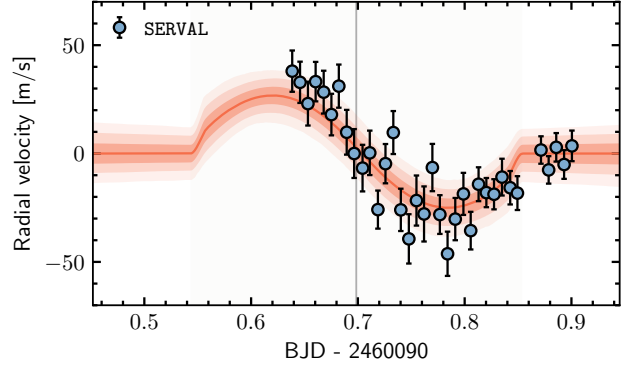
(b) In-transit RVs reduced by the SERVAL pipeline, which infer $\lambda = 10.9^{+11.8\circ}_{-11.5}$. The orbit trend has been subtracted.
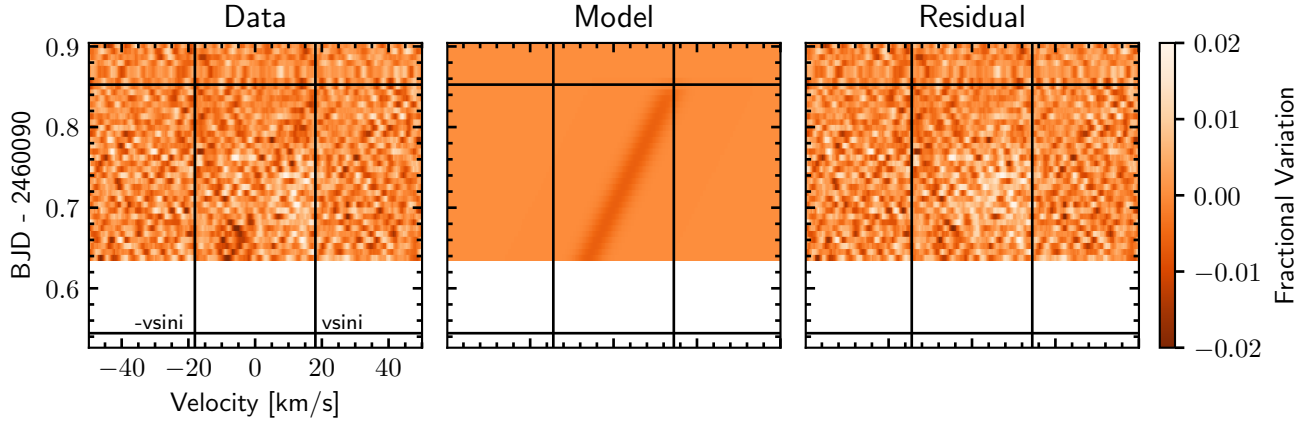
(c) Doppler Tomography signal, which infers $\lambda = 6.8^{+2.9\circ}_{-3.8}$.

Figure 2. NEID's first RM-effect visit on May 26th, 2023. Data was reduced by three different reduction techniques. The inferred projected stellar obliquities are consistent, but Doppler Tomography (DT) provides the tightest constraint. (a) and (b) In-transit radial-velocity measurements of the TOI-2145 system using the NEID spectra. The blue dots and black bars are NEID RVs and their corresponding uncertainties. The planet's transit and mid-transit time are indicated by the grey shaded region and grey vertical line, respectively. (c) The Doppler Tomography (planetary shadow) signal of the TOI-2145 system during TOI-2145b's transit. The left, middle, and right panels are data extracted from the NEID spectra, best-fit model, and the residual of the data after subtracting the best-fit model. The color scale presents the flux variation of the velocity channel.
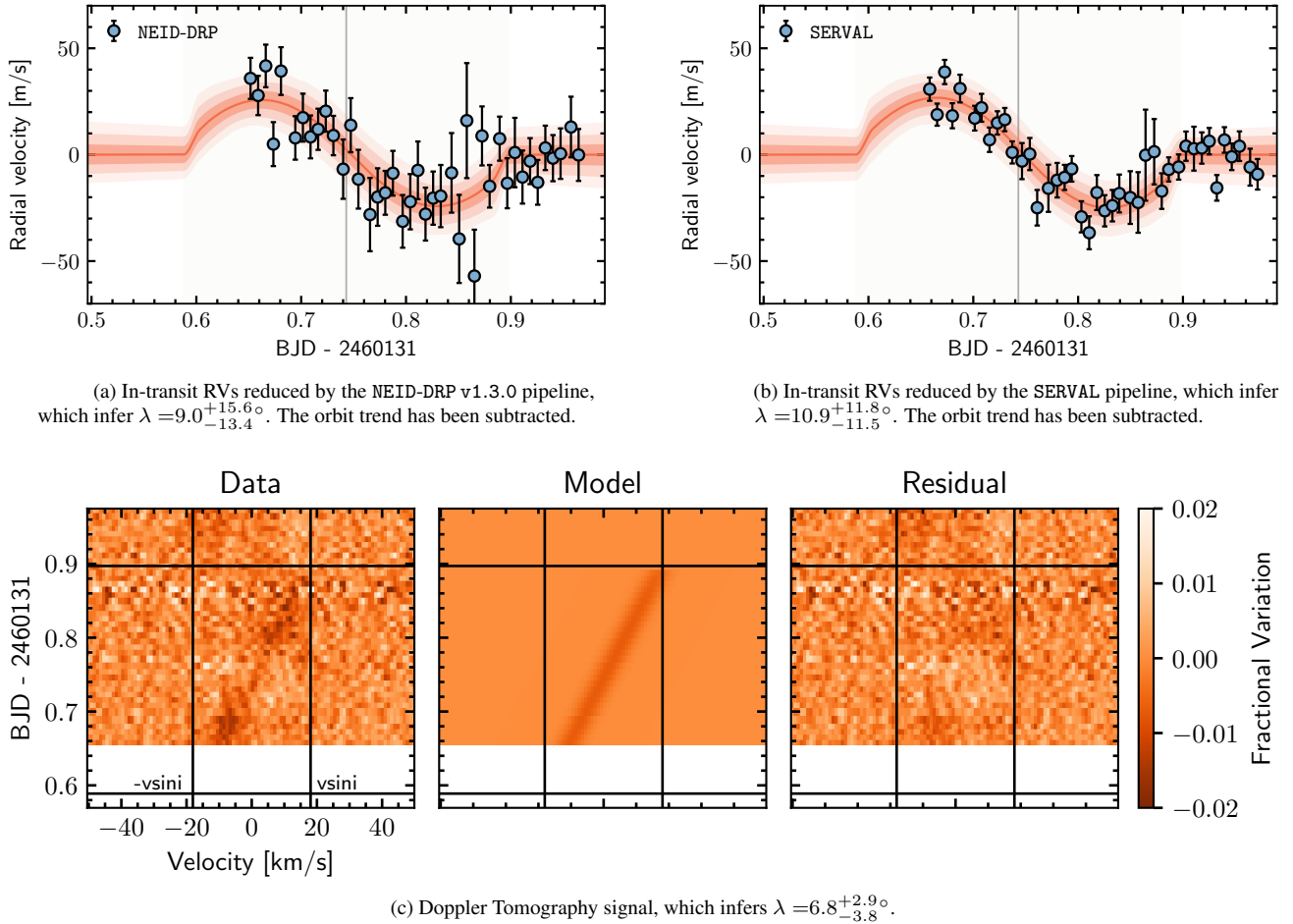
In summary, TOI-2145b is a $5.68^{+0.37}_{-0.34}\ M_{\rm Jup}$ planet on a moderately eccentric ($e_p = 0.214^{+0.014}_{-0.014}$), slightly misaligned ($\lambda = 6.8^{+2.9\circ}_{-3.8}$) orbit. The planet's orbital period is $P = 10.261128^{+0.000009}_{-0.000007}$-day, with a semi-major axis of $a = 0.1117^{+0.0035}_{-0.0034}$-au and a planet-star separation of $a/R_\star = 8.74^{+0.16}_{-0.14}$. The planet has a size of $R_p = 1.092^{+0.030}_{-0.028}\ R_{\rm Jup}$. The planet's mass, eccentricity, and radius are consistent with previous estimates (Rodriguez et al. 2023; Chontos et al. 2024).

In all three models, the HIRES RVs present high RV jitters in residuals, with an amplitude of $23\,{\rm m\,s^{-1}}$. We use the Gaussian process kernels for granulation and oscillations given in Luhn et al. (2023) to estimate the expected white-noise-equivalent levels of additional variability due to granulation and oscillations. The granulation kernel is composed of two Harvey-like components with frequencies and ampli-

tudes scaled by the effective temperature of 6206^{+81}_{-75} K and $\log g$ of 3.79 ± 0.02; the expected white-noise equivalent for granulation is $1.6\,{\rm m\,s^{-1}}$. The oscillations kernel is described by a stochastically driven, damped harmonic oscillator with frequency and amplitude scaled by ν_{max}; the expected white-noise equivalent for oscillations is $1.7\,{\rm m\,s^{-1}}$. The large RV jitters are likely due to the high $v \sin i_\star$ of the host star, which is $\sim 18\,{\rm km\,s^{-1}}$.

4.3. *Search for External Companions*

Next, we search for additional planets or stellar companions in the TOI-2145 system. Given TOI-2145b's high mass and eccentric orbit, its external perturbers could potentially be massive. Despite the long baseline of HIRES RVs, we find no clear evidence of additional companions in the RV residuals due to the large RV jitters caused by the fast rota-

(a) In-transit RVs reduced by the `NEID-DRP v1.3.0` pipeline, which infer $\lambda = 9.0^{+15.6}_{-13.4}{}^{\circ}$. The orbit trend has been subtracted.

(b) In-transit RVs reduced by the `SERVAL` pipeline, which infer $\lambda = 10.9^{+11.8}_{-11.5}{}^{\circ}$. The orbit trend has been subtracted.

(c) Doppler Tomography signal, which infers $\lambda = 6.8^{+2.9}_{-3.8}{}^{\circ}$.

Figure 3. Same as Figure 2, but for the NEID's second RM-effect visit on July 6th, 2023.

tion of the host star. The median RV residual is at a level of $12\,\mathrm{m\,s^{-1}}$, while the RV jitter combined with HIRES measurement uncertainty is about $24\,\mathrm{m\,s^{-1}}$.

The proper motion anomaly (PMa) technique is a powerful approach for searching for long-period, massive companions orbiting TOI-2145. This technique is based on identifying the difference between the long-term proper motion of the star, as measured by *Gaia* and *Hipparcos*, and the short-term proper motion recorded by *Gaia* alone (Brandt 2021; Kervella et al. 2022). The anomaly could indicate the presence of an external companion, though it is subject to degeneracy in mass and semimajor axis. We adopt the PMa for TOI-2145 (HIP 86040; Gaia DR3 1344163891352965632) from the Kervella et al. (2022) catalog. The star exhibits a tangential velocity anomaly of $66.5 \pm 44.8\,\mathrm{m\,s^{-1}}$. While the signal is insignificant, if the velocity anomaly of the star is indeed introduced by another planet, it could correspond to a $9 \pm 5\,M_{\mathrm{Jup}}$-mass planet at 5 au with mass-semimajor axis degeneracy. However, the contributions from stellar noise and instrumental systematics are not well understood, and thus the detection of the companion is inconclusive. Gaia

DR4 may provide more evidence on the existence of external companions.

We also check if TOI-2145 has a common proper motion (CPM) with any other stars from the Kervella et al. (2022) catalog. While a nearby star with a projected linear separation of 47100 au and a V-band magnitude of 15.9 is found, it receives a candidate companion score (P_{tot}) of 0.112 (see Section 3.4.3 of Kervella et al. (2022) for a detailed description of the metrics), indicating a low probability of being a co-moving or bound companion. The star is likely a nearby field star.

5. DISCUSSION

TOI-2145b is a 10.26-day, 5.7 ± 0.3 Jupiter-mass planet orbiting an evolved A star. The planet has a moderately eccentric orbit of $e = 0.21 \pm 0.01$. In this work, we combine *TESS* and previous HIRES observations (Chontos et al. 2024) with our new NEID RM-effect measurements to constrain the planet's orbital properties. We find that TOI-2145b has a nearly aligned orbit with a projected stellar obliquity of $\lambda = 6.8^{+2.9}_{-3.8}{}^{\circ}$. Given the current low orbital eccentricity of TOI-2145b, the planet is unlikely to be undergoing high-

eccentricity tidal migration unless it can excite its eccentricity to much higher values, for example, through secular interactions with other planets (Petrovich & Tremaine 2016). TOI-2145b more likely migrated inwards from the outer disk or formed in-situ. The observed orbital eccentricity and inclination of TOI-2145b is likely an outcome of the planet-disk interactions (Duffell & Chiang 2015) or post-formation dynamical evolution with other planets in the system.

The TOI-2145 system is interesting from multiple perspectives. First, TOI-2145b is a super Jupiter, a class of giant planets with masses beyond $\sim 2\,M_{\rm Jup}$ but still below the brown dwarf's deuterium fusion limit. Recently, Gupta et al. (2024) showed that these super Jupiters tend to have more eccentric orbits than their less massive counterparts, potentially as a result of planet-planet interactions. Thus, it is interesting to understand whether TOI-2145b is born with this mass or grows due to collisions. Second, TOI-2145b's orbit is nearly aligned with its host star spin axis. We discuss how spin-orbit coupling may play a role in the planet's orbital obliquity. Third, TOI-2145b's host star is evolved. Because of the inflation of the host star radius, its planet-star separation ($a/R_\star$) decreased by a factor of 2 from roughly 18 to 9. The inflation of the star could potentially increase the planet-star tidal interactions, speeding up the spin-orbit alignment or heating the atmosphere of TOI-2145b. However, we do not see an inflation of TOI-2145b's radius, likely due to the high surface gravity of the planet and also the relatively short timescale since the star evolved off the main sequence.

5.1. *Origins of Super Jupiters*

TOI-2145b is noteworthy for its substantial mass. As a super Jupiter with nearly six times the mass of Jupiter, it raises the question: Was it born with such a high mass, or did the planet acquire its mass through collisions between multiple planets? The observed positive mass-eccentricity relationship among warm, giant planets (Gupta et al. 2024) may suggest the latter scenario, especially when considering TOI-2145b within a population of warm Jupiters.

Confirming this hypothesis requires a detailed, population-level dynamical study. Here, we build toy models with N-body simulations to explore two formation scenarios. We consider a 4-planet system with the innermost planet having a semimajor axis of 0.1 au. While our understanding of the multiplicity of giant planets remains largely incomplete, RV surveys, such as the California Legacy Survey (CLS; Rosenthal et al. 2021), suggest that a significant fraction ($\sim$ 40%) of giant planets are in multiplanet systems (Zhu 2022). Moreover, the 4-planet setup facilitates the formation of super Jupiters through collisions between Jupiter-mass objects.

To construct the initial condition of a planetary system, we use three free parameters: the total mass of the four planets ($M_{\rm tot}$), the standard deviation of mass distribution among the four planets in the same system (σ_{m_p}), and the mutual Hill radii between neighboring planet pairs (Δa_p). The masses of the planets in the same system are drawn from a normal distribution with a mean of $M_{\rm tot}/4$ and a variance of σ_{m_p}. The initial eccentricity and inclination are assumed to be 0.01 for all planets. In all population synthesis simulations presented in this work, we assume σ_{m_p} follows a normal distribution with a mean of 1 and a standard deviation of 0.5 in the unit of Jupiter mass, bounded between 0 and 2. Δa_p follows a normal distribution with a mean of 4 and a standard deviation of 0.2. We vary the $M_{\rm tot}$ to explore how it determines the outcome of the planetary system architecture.

We consider a low disk mass scenario with a total planet mass $M_{\rm tot}$ following $\mathcal{N}(8, 1)$ and a high disk mass scenario with $M_{\rm tot} \sim \mathcal{N}(18, 1)$, both in units of Jupiter mass. We note that the definitions of low and high disk mass here are relative to each other in two scenarios. We simulate each system for 10 Myr using REBOUND with the IAS15 integrator (Rein & Liu 2012; Rein & Spiegel 2015). Collisions are checked at each timestep for crossing pathways using the line algorithm and resolved using the merge module, which conserves mass, momentum, and volume, but not energy. The realization of mass, orbital eccentricity, and inclination for the innermost warm Jupiter are shown in Figure 4. TOI-2145b is indicated by a red cross. Observed warm Jupiters are plotted in blue dots for reference.

For the low-disk mass case, as shown in the left panel of Figure 4, massive planets above 5 Jupiter masses are mostly grown through collisions, as is the case for TOI-2145b. These planets first have their eccentricities excited by interactions with other planets in the system, including scattering and ejection. Later on, collisions happen and tend to reduce the eccentricity of the planets. Planets between 2 and 5 Jupiter masses are also in systems with significant scattering and ejection, and thus experience eccentricity excitation. However, they have fewer mergers than those above 5 Jupiter masses. Planets below 2 Jupiter masses typically have low eccentricities; those with higher eccentricities are often dynamically unstable and get ejected. Collisions with the host star are rare. For the high-disk mass case, as shown in the right panel of Figure 4, massive planets are more common. For planets with a mass similar to TOI-2145b, scattering and ejection are still the dominant dynamical mechanisms to excite their eccentricities. Collisions, however, happen less frequently to these planets in the high-mass disk case than in the low-mass disk case. Therefore, super Jupiters born in low-mass disks and formed via collision are expected, on average, to have lower eccentricities than those born massive. A similar trend is observed in the inclination distribution, although it is less pronounced.

As shown by our simulations, TOI-2145b can be reproduced in both formation scenarios. It is plausible for the
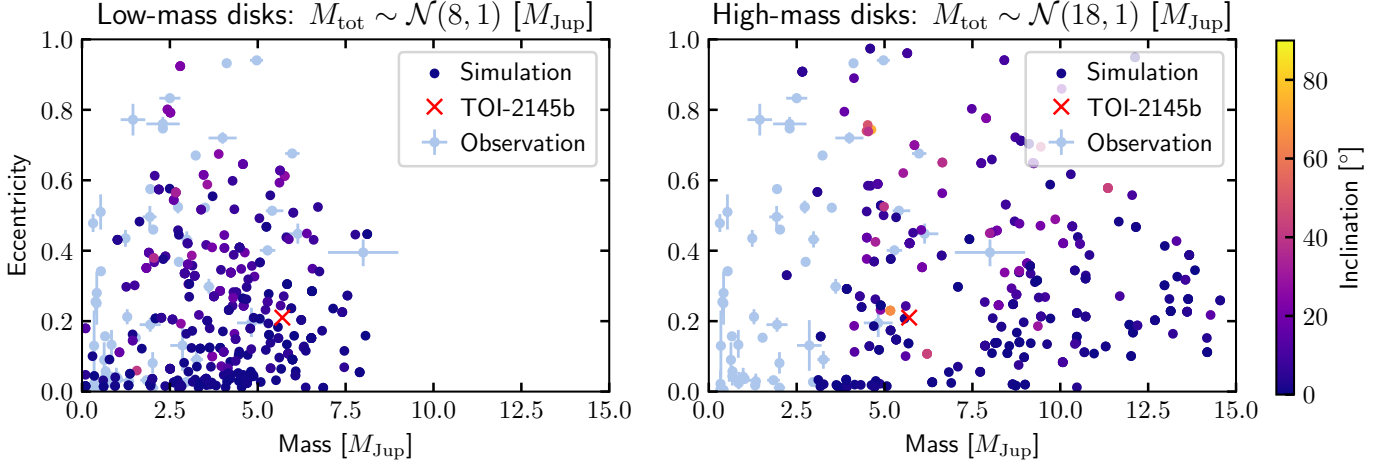
Figure 4. Mass and orbital properties of the innermost warm Jupiter in low-disk mass and high-disk mass scenarios. TOI-2145b is labeled as a red cross. Both planets born in a low-mass disk followed by collisions and in a high-mass disk followed by scatterings could explain the current properties of TOI-2145b.

planet to form from a low disk mass followed by collisions or from a massive disk with little or no collision. However, the two proposed scenarios for the formation of super Jupiters lead to distinct predictions about the overall eccentricity distribution of super Jupiters: super Jupiters born massive tend to have a broader eccentricity distribution than super Jupiters grown out of collisions. Based on existing observations of warm Jupiters, shown as blue dots in Figure 4, the collision scenario could provide a better match to the data. Additionally, our simulations show that super Jupiters formed through collisions are generally expected to have companions with masses similar to or lower than that of regular Jupiters, whereas those born with inherently high masses are likely to have companions with comparable masses. Consequently, searching for companion planets could be important in understanding the mass distribution within the system and determining which formation scenario is more plausible. This trend is based on the assumption of initial mass similarity among the planets, which will need to be examined in the future.

5.2. *Spin-Orbit Coupling of Close-in Planets*

TOI-2145b has joined the group of about two dozen warm Jupiters that have spin-orbit measurements, many of which show a tendency towards spin-orbit alignment around single stars (e.g., Rice et al. 2022; Dong et al. 2022; Espinoza-Retamal et al. 2023; Bieryla et al. 2024; Radzom et al. 2024; Wang et al. 2024). It is unclear if such a trend persists in binary systems. For example, TOI-1859b is a 64-day warm Jupiter with an eccentric and misaligned orbit ($e = 0.57^{+0.12}_{-0.16}$, $\lambda = 38.9^{+2.8°}_{-2.7}$), whose host star has a distant companion (Dong et al. 2023). The role of the binary companion in determining planet formation remains open for discussion. Here we discuss the importance of spin-orbit coupling and how it might affect stellar obliquity distribution.

The gravitational coupling between the close-in giant planet and its oblate host star may prevent the spin-orbit misalignment of the giant planet's orbit excited by the companion. Under the assumption of the dynamical perturbation of warm Jupiters happen mostly after they migrate at the current orbital distances, the external companion needs to overcome spin-orbit coupling from the star to excite the inner planet's inclination. Such an effect is the strongest around the fast rotating host stars, which could be TOI-2145 in this case. Lai et al. (2018) defined the planet-star coupling factor $\epsilon_{\star 1}$, where the smaller the value, the stronger coupling between the planet and the star, and the weaker the distant, external perturber to excite the inclination of the planet. Using Equation (24) in Lai et al. (2018), the planet-star coupling factor $\epsilon_{\star 1}$ follows

$$
\begin{aligned}
\epsilon_{\star 1} &= \frac{\omega_{12}}{\omega_{\star 1}} \left(\frac{1 - \omega_{\star 2}/\omega_{12}}{1 + S_\star/L_1} \right) \\
&\simeq 1.25 \left(\frac{6k_{q\star}}{k_\star} \right)^{-1} \frac{m_2}{m_1} \left(\frac{a_1}{0.04\,\mathrm{au}} \right)^{9/2} \left(\frac{\tilde{a}_2}{1\,\mathrm{au}} \right)^{-3} \left(\frac{P_\star}{30\,\mathrm{d}} \right) \\
&\times \left(\frac{M_\star}{M_\odot} \right)^{1/2} \left(\frac{R_\star}{R_\odot} \right)^{-3} \left(\frac{1}{1 + S_\star/L_1} \right),
\end{aligned}
\tag{1}
$$

where $S_\star/L_1$ is the ratio of stellar spin angular momentum and orbital angular momentum of the inner planet,

$$
\begin{aligned}
\frac{S_\star}{L_1} &= 0.079 \left(\frac{k_\star}{0.06} \right)^{-1} \left(\frac{m_1}{M_J} \right)^{-1} \left(\frac{a_1}{0.04\,\mathrm{au}} \right)^{-1/2} \left(\frac{P_\star}{30\,\mathrm{d}} \right)^{-1} \\
&\times \left(\frac{M_\star}{M_\odot} \right)^{1/2} \left(\frac{R_\star}{R_\odot} \right)^2.
\end{aligned}
\tag{2}
$$

Here, the notation $\star$ means the central star, 1 means the inner planet, and 2 means the distant perturber. ω_{xy} means the precession rate of x due to y. $k_{q\star}$ and $k_\star$ are the Love numbers of the star and the planet, m_1 and m_2 are the masses
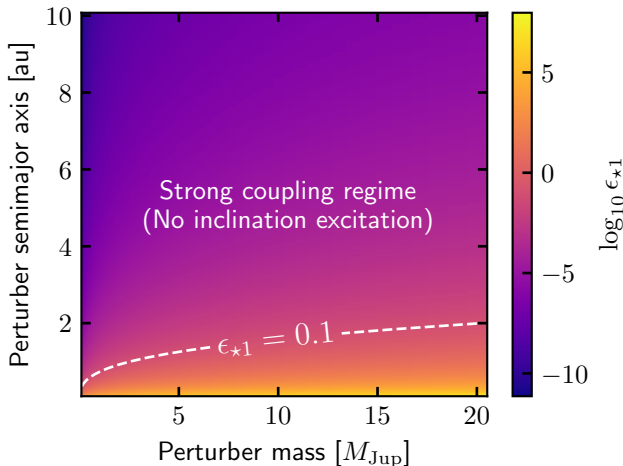
Figure 5. Spin-Orbit coupling factor $\epsilon_{\star 1}$ between TOI-2145 and TOI-2145b given different perturber properties. Here we assume a stellar rotation rate of 5 days. The dashed line corresponds to $\epsilon_{\star 1} = 0.1$. Perturbers above the line are unlikely to excite the mutual inclination of the inner planet due to spin-orbit coupling.

of the planet and the perturber, respectively, a_1 is the planet's semimajor axis, $\tilde{a}_2$ is the perturber's effective semimajor axis $\tilde{a}_2 = a_2\sqrt{1-e_2^2}$, $P_\star$ is the star's rotation period, and $M_\star$ and $R_\star$ are the star's mass and radius.

In Figure 5, we show how the star-planet coupling factor, $\epsilon_{\star 1}$, varies for a perturber with different masses and semimajor axes. If $\epsilon_{\star 1} \ll 1$, we consider the star-planet coupling is strong, and thus it is unlikely that the perturber will excite the inclination of the close-in giant planet. As shown in Figure 5, for a perturber with a semimajor axis greater than ~ 1–2 au, no matter of its mass, regardless of its mass, the inner planet is always in the strong spin-orbit coupling regime with the star, resulting in a consistently low stellar obliquity. For example, the hypothetical planet with a semimajor axis of 5 AU and a mass of 9 $M_{\rm Jup}$ inferred from the *Gaia* and *Hipparcos* proper motion anomalies, would be too distant from TOI-2145b to excite its inclination. If the perturber is close in ($a_2 \lesssim 1$ au), it may overcome the gravitational coupling. Although this is not indicated by the current stellar obliquity measurements, the existence of such a perturber could potentially be detected in long-term radial-velocity observations. However, the RV precision might be compromised due to the star's high $v \sin i_\star$.

5.3. *Stellar Obliquity of Evolved Stars*

The RM-effect observation around evolved stars is challenging due to the increased transit duration caused by stellar radius inflation. Notably, TOI-2145b has the longest orbital period among planets orbiting evolved stars for which an RM-effect measurement has been obtained. It joins a small population of planets, including WASP-71b (Smith et al. 2013; Brown et al. 2017), HAT-P-7b (Winn et al. 2009; Narita

et al. 2009; Albrecht et al. 2012; Lund et al. 2014), TOI-1181b (Saunders et al. 2024), TOI-4379b (Saunders et al. 2024), and TOI-6029b (Saunders et al. 2024). These planets have orbital periods ranging from 2–6 days and masses of a few Jupiter masses. Most of these planets, except HAT-P-7b, indicate a low stellar obliquity.

TOI-2145 is a hot star that had an effective temperature near or above the Kraft break before becoming a subgiant. While stellar evolution may decrease the planet-star separation ($a/R_\star$), thereby increasing star-planet interactions and speeding up the tidal realignment process, whether the planet had a spin-orbit misalignment before stellar evolution remains open for discussion. As discussed in the previous subsection, spin-orbit coupling between the star and the planet may prevent the excitation of TOI-2145b's mutual inclination relative to the perturber planet in the first place.

Table 1. Median values and 68% highest density intervals (HDI) for the stellar and planetary parameters of the TOI-2145 (TIC-88992642) system. The planetary and orbital parameters are derived from a joint fit of TESS transits, HIRES, and NEID radial velocities.

Parameter	Units	Values		
Stellar Properties				
$\alpha_{\rm J2016}$	*Gaia* DR3 RA (HH:MM:SS.ss)	17:35:01.94		
$\delta_{\rm J2016}$	*Gaia* DR3 Dec (DD:MM:SS.ss)..........	+40:41:42.15		
ϖ	*Gaia* DR3 parallax (mas)	4.420 ± 0.013		
G	*Gaia* DR3 G magnitude	8.9453		
$G_{\rm BP}$	*Gaia* DR3 $G_{\rm BP}$ magnitude	9.2178		
$G_{\rm RP}$	*Gaia* DR3 $G_{\rm RP}$ magnitude	8.5075		
$M_\star$	Stellar mass ($M_\odot$)......................	1.71 ± 0.04		
$R_\star$	Stellar radius ($R_\odot$)	$2.75^{+0.06}_{-0.05}$		
$\rho_\star$	Stellar density ($\rho_\odot$).....................	0.081 ± 0.005		
$\log g$	Stellar surface gravity (cgs)..............	3.79 ± 0.02		
$T_{\rm eff}$	Stellar effective temperature (K)	6206^{+81}_{-75}		
[m/H]	Stellar bulk metallicity (dex).............	$+0.28^{+0.06}_{-0.05}$		
Age	Stellar age (Gyr)........................	$1.6^{+0.2}_{-0.1}$		
$v \sin i_{\star,\rm spec}$...	Spectral projected line broadening (km s^{-1})	17.8 ± 1.0		
Planetary and Orbital Properties				
		With DT	With SERVAL	With NEID-DRP
P	Period (days)...........................	$10.261128^{+0.000009}_{-0.000007}$	$10.261132^{+0.000008}_{-0.000008}$	$10.261131^{+0.000008}_{-0.000008}$
T_C	Mid-transit time (BJD-2457000)	$1982.49662^{+0.00055}_{-0.00054}$	$1982.49655^{+0.00053}_{-0.00055}$	$1982.49656^{+0.00052}_{-0.00054}$
a	Semi-major axis (au).....................	$0.1117^{+0.0035}_{-0.0034}$	$0.1095^{+0.0030}_{-0.0033}$	$0.1098^{+0.0035}_{-0.0031}$
$a/R_\star$	Planet-star separation	$8.74^{+0.16}_{-0.14}$	$8.58^{+0.14}_{-0.13}$	$8.60^{+0.17}_{-0.15}$
b	Impact parameter	$0.165^{+0.069}_{-0.082}$	$0.168^{+0.108}_{-0.104}$	$0.192^{+0.124}_{-0.106}$
i	Orbital inclination (°)	$88.6^{+0.7}_{-0.6}$	$88.6^{+1.1}_{-0.7}$	$88.4^{+1.0}_{-1.0}$
$R_p/R_\star$	Planet-star radius ratio	$0.04082^{+0.00024}_{-0.00027}$	$0.04099^{+0.00026}_{-0.00029}$	$0.04101^{+0.00029}_{-0.00029}$
R_p	Planet radius ($R_{\rm Jup}$)	$1.092^{+0.030}_{-0.027}$	$1.097^{+0.028}_{-0.026}$	$1.098^{+0.026}_{-0.028}$
M_p	Planet mass ($M_{\rm Jup}$).....................	$5.68^{+0.37}_{-0.34}$	$5.51^{+0.31}_{-0.35}$	$5.52^{+0.35}_{-0.34}$
e	Orbital eccentricity	$0.214^{+0.014}_{-0.014}$	$0.230^{+0.011}_{-0.012}$	$0.224^{+0.013}_{-0.013}$
ω	Argument of periapse (°)	$96.2^{+2.4}_{-2.5}$	$95.9^{+2.4}_{-2.4}$	$96.0^{+2.4}_{-2.3}$
λ	Projected stellar obliquity (°)	$6.8^{+2.9}_{-3.8}$	$10.9^{+11.8}_{-11.5}$	$9.0^{+15.6}_{-13.4}$
Other Parameters in the Joint Model				
$v \sin i_\star$	Fitted projected line broadening (km s^{-1})..	$18.06^{+0.36}_{-0.39}$	$18.61^{+0.78}_{-0.95}$	$18.39^{+0.94}_{-0.88}$
$\sigma_{\rm RV,HIRES}$ ...	HIRES RV jitter (m s^{-1})	$23.2^{+2.3}_{-2.8}$	$23.5^{+2.4}_{-2.7}$	$23.3^{+2.5}_{-2.7}$
$v_{\rm macro,v1}$	Host star macroturbulence, visit 1 (km s^{-1})	$2.64^{+0.20}_{-0.23}$	-	-
$v_{\rm macro,v2}$	Host star macroturbulence, visit 2 (km s^{-1})	$2.34^{+0.20}_{-0.21}$	-	-
$\sigma_{\rm RV,SERVAL,v1}$	SERVAL RV jitter, visit 1 (m s^{-1})..........	-	$5.9^{+1.6}_{-2.0}$	-
$\sigma_{\rm RV,SERVAL,v2}$	SERVAL RV jitter, visit 2 (m s^{-1})..........	-	$4.8^{+1.3}_{-1.3}$	-
$\sigma_{\rm RV,DRP,v1}$ ...	NEID-DRP RV jitter, visit 1 (m s^{-1})........	-	-	$8.4^{+2.3}_{-2.7}$
$\sigma_{\rm RV,DRP,v2}$ ...	NEID-DRP RV jitter, visit 2 (m s^{-1})........	-	-	$6.1^{+1.6}_{-2.1}$

NOTE—*Gaia* magnitudes and spectral line broadening parameter are obtained from the *Gaia* Data Release 3 (Gaia Collaboration et al. 2021). Both NEID RM-effect observations are included in the joint fit. Planetary parameters inferred from the Doppler Tomography signal are used for discussion.

SPOC data products. The TESS data presented in this paper were obtained from the MAST at the Space Telescope Science Institute. The specific observations analyzed can be accessed via 10.17909/t9-nmc8-f686 and 10.17909/t9-st5g-3177. The TESS Input Catalog and Candidate Target List can be accessed via 10.17909/fwdt-2x66. This work has made use of data from the European Space Agency (ESA) mission *Gaia* (https://www.cosmos.esa.int/gaia), processed by the *Gaia* Data Processing and Analysis Consortium (DPAC, https://www.cosmos.esa.int/web/gaia/dpac/consortium).

Data presented were obtained by the NEID spectrograph built by Penn State University and operated at the WIYN Observatory by NOIRLab, under the NN-EXPLORE partnership of the National Aeronautics and Space Administration and the National Science Foundation. These results are based on observations obtained with NEID on the WIYN 3.5m Telescope at Kitt Peak National Observatory (co-PIs: Ashley Chontos & Jiayin Dong, NOIRLab 2023A-652300). WIYN is a joint facility of the University of Wisconsin–Madison, Indiana University, NSF's NOIRLab, the Pennsylvania State University, Purdue University, University of California, Irvine, and the University of Missouri. The authors are honored to be permitted to conduct astronomical research on Iolkam Du'ag (Kitt Peak), a mountain with particular significance to the Tohono O'odham.

This research made use of exoplanet (Foreman-Mackey et al. 2019; Foreman-Mackey et al. 2021) and its dependencies (Agol et al. 2020; Astropy Collaboration et al. 2013, 2018; Foreman-Mackey et al. 2019; Foreman-Mackey et al. 2017; Foreman-Mackey 2018; Kipping 2013b; Luger et al. 2019; Wiecki et al. 2022).

Facilities: TESS, *Gaia*, WIYN/NEID, Keck/HIRES, Exoplanet Archive

Software: ArviZ (Kumar et al. 2019), astropy (Astropy Collaboration et al. 2013, 2018), celerite2 (Foreman-Mackey et al. 2017; Foreman-Mackey 2018), exoplanet (Foreman-Mackey et al. 2021; Foreman-Mackey et al. 2019), Jupyter (Kluyver et al. 2016), Matplotlib (Hunter 2007; Droettboom et al. 2016), NumPy (van der Walt et al. 2011; Harris et al. 2020), pandas (Wes McKinney 2010; pandas development team 2020), PyMC (Wiecki et al. 2022), SciPy (Virtanen et al. 2020), Tapir (Jensen 2013)

REFERENCES

Agol, E., Luger, R., & Foreman-Mackey, D. 2020, AJ, 159, 123, doi: 10.3847/1538-3881/ab4fee

Albrecht, S., Winn, J. N., Johnson, J. A., et al. 2012, ApJ, 757, 18, doi: 10.1088/0004-637X/757/1/18

Anderson, K. R., Lai, D., & Pu, B. 2020, MNRAS, 491, 1369, doi: 10.1093/mnras/stz3119

Astropy Collaboration, Robitaille, T. P., Tollerud, E. J., et al. 2013, A&A, 558, A33, doi: 10.1051/0004-6361/201322068

Astropy Collaboration, Price-Whelan, A. M., Sipőcz, B. M., et al. 2018, AJ, 156, 123, doi: 10.3847/1538-3881/aabc4f

Bieryla, A., Zhou, G., García-Mejía, J., et al. 2024, MNRAS, 527, 10955, doi: 10.1093/mnras/stad3785

Boisse, I., Eggenberger, A., Santos, N. C., et al. 2010, A&A, 523, A88, doi: 10.1051/0004-6361/201014909

Brandt, T. D. 2021, ApJS, 254, 42, doi: 10.3847/1538-4365/abf93c

Brown, D. J. A., Triaud, A. H. M. J., Doyle, A. P., et al. 2017, MNRAS, 464, 810, doi: 10.1093/mnras/stw2316

Butler, R. P., Wright, J. T., Marcy, G. W., et al. 2006, ApJ, 646, 505, doi: 10.1086/504701

Castelli, F., & Kurucz, R. L. 2004, ArXiv Astrophysics e-prints

Chaplin, W. J., Cegla, H. M., Watson, C. A., Davies, G. R., & Ball, W. H. 2019, AJ, 157, 163, doi: 10.3847/1538-3881/ab0c01

Chatterjee, S., Ford, E. B., Matsumura, S., & Rasio, F. A. 2008, ApJ, 686, 580, doi: 10.1086/590227

Choi, J., Dotter, A., Conroy, C., et al. 2016, ApJ, 823, 102, doi: 10.3847/0004-637X/823/2/102

Chontos, A., Huber, D., Grunblatt, S. K., et al. 2024, arXiv e-prints, arXiv:2402.07893, doi: 10.48550/arXiv.2402.07893

Collier Cameron, A., Guenther, E., Smalley, B., et al. 2010, MNRAS, 407, 507, doi: 10.1111/j.1365-2966.2010.16922.x

Collins, K., Quinn, S. N., Latham, D. W., et al. 2018, in American Astronomical Society Meeting Abstracts, Vol. 231, American Astronomical Society Meeting Abstracts #231, 439.08

Donati, J.-F., Semel, M., Carter, B. D., Rees, D. E., & Collier Cameron, A. 1997, MNRAS, 291, 658, doi: 10.1093/mnras/291.4.658

Dong, J., Huang, C. X., Dawson, R. I., et al. 2021, ApJS, 255, 6, doi: 10.3847/1538-4365/abf73c

Dong, J., Huang, C. X., Zhou, G., et al. 2022, ApJL, 926, L7, doi: 10.3847/2041-8213/ac4da0

Dong, J., Wang, S., Rice, M., et al. 2023, ApJL, 951, L29, doi: 10.3847/2041-8213/acd93d

Dotter, A. 2016, ApJS, 222, 8, doi: 10.3847/0067-0049/222/1/8

Droettboom, M., Hunter, J., Caswell, T. A., et al. 2016, Matplotlib: Matplotlib V1.5.1, v1.5.1, Zenodo, doi: 10.5281/zenodo.44579

Duffell, P. C., & Chiang, E. 2015, ApJ, 812, 94, doi: 10.1088/0004-637X/812/2/94

Espinoza-Retamal, J. I., Brahm, R., Petrovich, C., et al. 2023, ApJL, 958, L20, doi: 10.3847/2041-8213/ad096d

Ford, E. B., & Rasio, F. A. 2008, ApJ, 686, 621,
    doi: 10.1086/590926

Foreman-Mackey, D. 2018, Research Notes of the American
    Astronomical Society, 2, 31, doi: 10.3847/2515-5172/aaaf6c

Foreman-Mackey, D., Agol, E., Ambikasaran, S., & Angus, R.
    2017, AJ, 154, 220, doi: 10.3847/1538-3881/aa9332

Foreman-Mackey, D., Czekala, I., Luger, R., et al. 2019,
    dfm/exoplanet: exoplanet v0.2.1, doi: 10.5281/zenodo.3462740

Foreman-Mackey, D., Luger, R., Agol, E., et al. 2021, arXiv
    e-prints, arXiv:2105.01994. https://arxiv.org/abs/2105.01994

Frelikh, R., Jang, H., Murray-Clay, R. A., & Petrovich, C. 2019,
    ApJL, 884, L47, doi: 10.3847/2041-8213/ab4a7b

Gaia Collaboration, Brown, A. G. A., Vallenari, A., et al. 2021,
    A&A, 649, A1, doi: 10.1051/0004-6361/202039657

Gelman, A., Carlin, J. B., Stern, H. S., et al. 2014, Bayesian Data
    Analysis

Gelman, A., & Rubin, D. B. 1992, Statistical Science, 7, 457,
    doi: 10.1214/ss/1177011136

Gupta, A. F., Millholland, S. C., Im, H., et al. 2024, Nature,
    doi: 10.1038/s41586-024-07688-3

Halverson, S., Terrien, R., Mahadevan, S., et al. 2016, in
    Proc. SPIE, Vol. 9908, Ground-based and Airborne
    Instrumentation for Astronomy VI, 99086P,
    doi: 10.1117/12.2232761

Harris, C. R., Jarrod Millman, K., van der Walt, S. J., et al. 2020,
    arXiv e-prints, arXiv:2006.10256.
    https://arxiv.org/abs/2006.10256

Hayward, T. L., Brandl, B., Pirger, B., et al. 2001, PASP, 113, 105,
    doi: 10.1086/317969

Henden, A. A., Levine, S., Terrell, D., & Welch, D. L. 2015, in
    American Astronomical Society Meeting Abstracts, Vol. 225,
    American Astronomical Society Meeting Abstracts #225, 336.16

Hirano, T., Suto, Y., Winn, J. N., et al. 2011, ApJ, 742, 69,
    doi: 10.1088/0004-637X/742/2/69

Huang, C. X., Vanderburg, A., Pál, A., et al. 2020a, Research
    Notes of the American Astronomical Society, 4, 204,
    doi: 10.3847/2515-5172/abca2e

—. 2020b, Research Notes of the American Astronomical Society,
    4, 206, doi: 10.3847/2515-5172/abca2d

Huber, D., Zinn, J., Bojsen-Hansen, M., et al. 2017, ApJ, 844, 102,
    doi: 10.3847/1538-4357/aa75ca

Hunter, J. D. 2007, Computing in Science and Engineering, 9, 90,
    doi: 10.1109/MCSE.2007.55

Jenkins, J. M., Twicken, J. D., McCauliff, S., et al. 2016, in Society
    of Photo-Optical Instrumentation Engineers (SPIE) Conference
    Series, Vol. 9913, Software and Cyberinfrastructure for
    Astronomy IV, ed. G. Chiozzi & J. C. Guzman, 99133E,
    doi: 10.1117/12.2233418

Jensen, E. 2013, Tapir: A web interface for transit/eclipse
    observability, Astrophysics Source Code Library.
    http://ascl.net/1306.007

Jurić, M., & Tremaine, S. 2008, ApJ, 686, 603,
    doi: 10.1086/590047

Kanodia, S., Mahadevan, S., Ramsey, L. W., et al. 2018, in Society
    of Photo-Optical Instrumentation Engineers (SPIE) Conference
    Series, Vol. 10702, Ground-based and Airborne Instrumentation
    for Astronomy VII, ed. C. J. Evans, L. Simard, & H. Takami,
    107026Q, doi: 10.1117/12.2313491

Kanodia, S., Lin, A. S. J., Lubar, E., et al. 2023, AJ, 166, 105,
    doi: 10.3847/1538-3881/acea60

Kervella, P., Arenou, F., & Thévenin, F. 2022, A&A, 657, A7,
    doi: 10.1051/0004-6361/202142146

Kipping, D. M. 2013a, MNRAS, 435, 2152,
    doi: 10.1093/mnras/stt1435

—. 2013b, MNRAS, 435, 2152, doi: 10.1093/mnras/stt1435

Kluyver, T., Ragan-Kelley, B., Pérez, F., et al. 2016, in Positioning
    and Power in Academic Publishing: Players, Agents and
    Agendas, ed. F. Loizides & B. Scmidt (Netherlands: IOS Press),
    87–90. https://eprints.soton.ac.uk/403913/

Kumar, R., Carroll, C., Hartikainen, A., & Martin, O. 2019, Journal
    of Open Source Software, 4, 1143, doi: 10.21105/joss.01143

Lai, D., Anderson, K. R., & Pu, B. 2018, MNRAS, 475, 5231,
    doi: 10.1093/mnras/sty133

Luger, R., Agol, E., Foreman-Mackey, D., et al. 2019, AJ, 157, 64,
    doi: 10.3847/1538-3881/aae8e5

Luhn, J. K., Ford, E. B., Guo, Z., et al. 2023, AJ, 165, 98,
    doi: 10.3847/1538-3881/acad08

Lund, M. N., Lundkvist, M., Silva Aguirre, V., et al. 2014, A&A,
    570, A54, doi: 10.1051/0004-6361/201424326

Narita, N., Sato, B., Hirano, T., & Tamura, M. 2009, PASJ, 61,
    L35, doi: 10.1093/pasj/61.5.L35

Oriol, A.-P., Virgile, A., Colin, C., et al. 2023, PeerJ Computer
    Science, 9, e1516, doi: 10.7717/peerj-cs.1516

pandas development team, T. 2020, pandas-dev/pandas: Pandas,
    latest, Zenodo, doi: 10.5281/zenodo.3509134

Petigura, E. A. 2015, PhD thesis, University of California,
    Berkeley

Petrovich, C., & Tremaine, S. 2016, ApJ, 829, 132,
    doi: 10.3847/0004-637X/829/2/132

Radzom, B. T., Dong, J., Rice, M., et al. 2024, arXiv e-prints,
    arXiv:2404.06504, doi: 10.48550/arXiv.2404.06504

Rein, H., & Liu, S. F. 2012, A&A, 537, A128,
    doi: 10.1051/0004-6361/201118085

Rein, H., & Spiegel, D. S. 2015, MNRAS, 446, 1424,
    doi: 10.1093/mnras/stu2164

Rice, M., Wang, S., Wang, X.-Y., et al. 2022, AJ, 164, 104,
    doi: 10.3847/1538-3881/ac8153

Ricker, G. R., Winn, J. N., Vanderspek, R., et al. 2014, in Society of Photo-Optical Instrumentation Engineers (SPIE) Conference Series, Vol. 9143, Space Telescopes and Instrumentation 2014: Optical, Infrared, and Millimeter Wave, ed. J. Oschmann, Jacobus M., M. Clampin, G. G. Fazio, & H. A. MacEwen, 914320, doi: 10.1117/12.2063489

Robertson, P., Anderson, T., Stefansson, G., et al. 2019, Journal of Astronomical Telescopes, Instruments, and Systems, 5, 015003, doi: 10.1117/1.JATIS.5.1.015003

Rodriguez, J. E., Quinn, S. N., Vanderburg, A., et al. 2023, MNRAS, 521, 2765, doi: 10.1093/mnras/stad595

Rosenthal, L. J., Fulton, B. J., Hirsch, L. A., et al. 2021, ApJS, 255, 8, doi: 10.3847/1538-4365/abe23c

Saunders, N., Grunblatt, S. K., Chontos, A., et al. 2024, AJ, 168, 81, doi: 10.3847/1538-3881/ad543b

Schwab, C., Rakich, A., Gong, Q., et al. 2016, in Proc. SPIE, Vol. 9908, Ground-based and Airborne Instrumentation for Astronomy VI, 99087H, doi: 10.1117/12.2234411

Skrutskie, M. F., Cutri, R. M., Stiening, R., et al. 2006, AJ, 131, 1163, doi: 10.1086/498708

Smith, A. M. S., Anderson, D. R., Bouchy, F., et al. 2013, A&A, 552, A120, doi: 10.1051/0004-6361/201220727

Stefansson, G., Hearty, F., Robertson, P., et al. 2016, ApJ, 833, 175, doi: 10.3847/1538-4357/833/2/175

Stefànsson, G., Mahadevan, S., Petrovich, C., et al. 2022, ApJL, 931, L15, doi: 10.3847/2041-8213/ac6e3c

Swift, J. J., Bottom, M., Johnson, J. A., et al. 2015, Journal of Astronomical Telescopes, Instruments, and Systems, 1, 027002, doi: 10.1117/1.JATIS.1.2.027002

van der Walt, S., Colbert, S. C., & Varoquaux, G. 2011, Computing in Science and Engineering, 13, 22, doi: 10.1109/MCSE.2011.37

Virtanen, P., Gommers, R., Oliphant, T. E., et al. 2020, Nature Methods, 17, 261, doi: 10.1038/s41592-019-0686-2

Vogt, S. S., Allen, S. L., Bigelow, B. C., et al. 1994, in Society of Photo-Optical Instrumentation Engineers (SPIE) Conference Series, Vol. 2198, Instrumentation in Astronomy VIII, ed. D. L. Crawford & E. R. Craine, 362, doi: 10.1117/12.176725

Wang, X.-Y., Rice, M., Wang, S., et al. 2024, ApJL, 973, L21, doi: 10.3847/2041-8213/ad7469

Wes McKinney. 2010, in Proceedings of the 9th Python in Science Conference, ed. Stéfan van der Walt & Jarrod Millman, 56 – 61, doi: 10.25080/Majora-92bf1922-00a

Wiecki, T., Salvatier, J., Patil, A., et al. 2022, pymc-devs/pymc:, v4.1.7, Zenodo, Zenodo, doi: 10.5281/zenodo.7467113

Wilson, M. L., Eastman, J. D., Cornachione, M. A., et al. 2019, PASP, 131, 115001, doi: 10.1088/1538-3873/ab33c5

Winn, J. N., Johnson, J. A., Albrecht, S., et al. 2009, ApJL, 703, L99, doi: 10.1088/0004-637X/703/2/L99

Wright, J. T., Upadhyay, S., Marcy, G. W., et al. 2009, ApJ, 693, 1084, doi: 10.1088/0004-637X/693/2/1084

Wu, D.-H., Rice, M., & Wang, S. 2023, AJ, 165, 171, doi: 10.3847/1538-3881/acbf3f

Zechmeister, M., Reiners, A., Amado, P. J., et al. 2018, A&A, 609, A12, doi: 10.1051/0004-6361/201731483

Zhu, W. 2022, AJ, 164, 5, doi: 10.3847/1538-3881/ac6f59